Mean flow characteristics of two-dimensional wings in ground effect

Jae Hwan Jung[1], Hyun Sik Yoon[2], Ho Hwan Chun[1], Pham Anh Hung[1] and Osama Ahmed Elsamni[3]

[1]*Department of Naval Architecture and Ocean Engineering, Pusan National University, Busan, Korea*
[2]*Global Core Research Center for Ships and Offshore Plants, Pusan National University, Busan, Korea*
[3]*Country Department of Mechanical Power Engineering, The University of Alexandra. El-Chatby, Alexandra, Egypt*

ABSTRACT: *The present study numerically investigates the aerodynamic characteristics of two-dimensional wings in the vicinity of the ground by solving two-dimensional steady incompressible Navier-Stokes equations with the turbulence closure model of the realizable $k - \varepsilon$ model. Numerical simulations are performed at a wide range of the normalized ground clearance by the chord length ($0.1 \leq h/C \leq 1.25$) for the angles of attack ($0° \leq \alpha \leq 10°$) in the pre-stall regime at a Reynolds number (Re) of 2×10^6 based on free stream velocity U_∞ and the chord length. As the physical model of this study, a cambered airfoil of NACA 4406 has been selected by a performance test for various airfoils. The maximum lift-to-drag ratio is achieved at $\alpha = 4°$ and $h/C = 0.1$. Under the conditions of $\alpha = 4°$ and $h/C = 0.1$, the effect of the Reynolds number on the aerodynamic characteristics of NACA 4406 is investigated in the range of $2 \times 10^5 \leq Re \leq 2 \times 10^9$. As Re increases, C_l and C_d augments and decreases, respectively, and the lift-to-drag ratio increases linearly.*

KEY WORDS: Wing; Ground effect; Ground clearances; Drag; Lift; Reynolds number effect.

INTRODUCTION

The aerodynamic characteristics of a wing in ground (WIG) effect craft is of special interests because of its wide applications not only during landing and take-off of airplanes but also for high speed water vehicle. When the wing with the small angles of attack operates in the proximity of the ground, the favorable aerodynamic characteristics can be achieved, which had been revealed by early researches, Raymond (1921) and Reid (1927). The lift increases by a high-pressure air cushion under the wing and the drag decreases due to the reduction of the downwash velocity, Recant (1939) and Seerebrisky (1946). Consequently, the lift-to-drag ratio generally representing the efficiency of an airplane becomes higher, as a result that the flight range of a WIG vehicle is wider than that of a conventional airplane for a given energy consumption.

Owing to these advantages of WIG vehicles, for several decades, various studies have been performed for two and three dimensional steady/unsteady numerical analysis of WIG by Nuhait and Mook (1989), Mizutani and Suzuki (1993), Hsiun and Chen (1995, 1996), Han, Cho and Cho (2005), Moon, Oh and Seo (2005); experimental studies by Fink and Lastinger (1996), Kim, Suh, Lee and Kim (1997), Zerihan and Zhang (2000), Ahmed and Goonaratne (2002), Zhang, Zerihan, Ruhrmann and Deviese (2002); the development of a WIG craft by Shin, et al. (1997), Chun, Chang, Paik and Chang (1997); the stability analysis by Chun and Chang (2002).

Recently, Ahmed and Sharma (2005) summarized well the experimental investigations into this problem. These studies have aimed at revealing the dependence of forces acting on the different wing configurations on the ground clearance. They have also concerned with understanding the WIG effect on the aerodynamic characteristics by experimentally examining the flow around a symmetrical airfoil of NACA 0015 with various angles of attack from 0° to 10° for the clearance varying from

Corresponding author: *Hyun-Sik Yoon*
e-mail: *lesmodel@pusan.ac.kr*

the minimum possible value to one chord length. They showed that high values of pressure coefficients appears on the lower surface with decreasing the ground clearance, leading to high lift when the wing is close to the ground. Their results suggested that the pressure distribution on the upper surface does not change significantly regardless of the variation of the ground clearance at higher incident angles.

The other investigative tools of the aerodynamic characteristics of WIG are the theoretical and numerical methods. However, most of previous theoretical and numerical researches focused on the inviscid flow by using the panel method or lifting surface model.

In contrast to the inviscid flow, Hsiun and Chen (1995, 1996) numerically considered the steady two-dimensional WIG in the laminar viscous flow. They concluded that the airfoil with larger camber and smaller thickness give a higher lift-to-drag ratio.

Moon, Oh and Seo (2005) numerically investigated three-dimensional cambered wing of NACA 4406 with 2 *degrees* angle of attack in ground effect for the aero-levitation electric vehicle at the Reynolds number of 2×10^6 based on the chord length by solving three-dimensional incompressible Navier-Stokes equations with the turbulence closure model. They focused on the flow structure according to the configuration of the main and vertical wings by which the high lift-to-drag ratio changes.

Recently, Kim, et al. (2006) numerically investigated two dimensional turbulent flow simulations on the low Mach number - high Reynolds number flow about the NACA 4412 airfoil are carried out as the airfoil approaches a ground. It has turned out that angle of attack between 2 and 8 *degrees* is recommended for the airfoil to utilize the benefit of ground effect. For the large angle of attack, the increment of lift due to the ground effect is faded away and negative aerodynamic effect such as destabilizing aspect in static longitudinal stability occurs and the separation point moves to forward as the airfoil approaches a ground.

Although a great deal of computational research has investigated the WIG problem, only a few studies have considered the viscous flow and especially the turbulence model for the nature of a high Reynolds number. Thus, the present study numerically investigates the aerodynamic characteristics of two-dimensional wings in the vicinity of the ground by solving two-dimensional steady incompressible Navier-Stokes equations with the turbulence closure model. Under the present conditions, it is difficult to accurately capture a stall angle of attack and resolve relatively large and highly complex vortical structures, especially in the post-stall regime. This difficulty in accurately simulating the post-stall regime was pointed out by several authors such as Ravindran (1999). Consequently, the present study focused on the mean flow characteristics in pre-stall regime.

For the systematical research, this work proceeds through the following steps. First, the aerodynamics characteristics of various two-dimensional NACA four-digit profiles are examined by considering their camber and thickness effects in order to select the one airfoil profile which gives a better performance in ground effect. Second, regarding the selected profile, the effect of the ground clearance ranging from 0.1 of the chord length to 1.25 of the chord length is investigated for various angles of attack from $0°$ to $10°$ on the aerodynamic characteristics. Finally, for the specified conditions of the ground clearance and the angle of attack where the highest value of the lift-to-drag ratio is obtained, the effect of the Reynolds number on the aerodynamic characteristics is researched, since the survey of the literature suggests that the WIG problem needs to be carried out for a high Reynolds number.

COMPUTATIONAL DETAILS

The commercial CFD package, FLUENT (2009), is employed for all numerical predictions. The present study considers the two-dimensional WIG problem with the assumption of the steady incompressible viscous flow in order to simplify the physical problem. Therefore, the governing equations describing the steady incompressible viscous flow field in the present study are the continuity and Reynolds averaged Navier-Stokes equations:

$$\frac{\partial U_i}{\partial x_i} = 0 \tag{1}$$

$$\frac{\partial}{\partial x_j}\left(\rho U_i U_j\right) = -\frac{\partial P}{\partial x_i} + \frac{\partial}{\partial x_j}\left[\mu\left(\frac{\partial U_i}{\partial x_j} + \frac{\partial U_j}{\partial x_i}\right)\right] + \frac{\partial}{\partial x_j}\left(-\rho\overline{u_i' u_j'}\right) \tag{2}$$

where x_i are Cartesian coordinates, U_i are the corresponding velocity components, ρ is the density, μ is the viscosity, and

P is the pressure. Also, $-\rho \overline{u_i' u_j'}$ in equation (2) is the Reynolds stress term which has been closed by using the realizable $k-\varepsilon$ model. The realizable $k-\varepsilon$ model is employed as the turbulence model, because of its improved predictive capabilities compared to the standard $k-\varepsilon$ model, and because of its ability to resolve portions of complex flows located very close to the surface. This model ensures that the turbulent normal stresses are always positive, which is consistent with the physics of complex turbulent flows. The standard wall function proposed by Launder and Spalding (1974) has been adopted to account for the overall resistance of the sublayer to momentum. With this scheme, the Reynolds averaged Navier-Stokes equations are solved numerically, in conjunction with transport equations for the turbulent kinetic energy and dissipation rate. The equations are solved by the SIMPLE algorithm with a second-order spatial discretization scheme based on a finite volume method. The convergence criterion of 10^{-4} has been used for the present simulations. Further details of the implementation can be found in the FLUENT (2009) manuals.

Fig. 1(a) shows the physical model of the two-dimensional WIG problem, the size of the computational domain and the coordinate system. The chord length of the wing is represented by C and the normalized ground clearance between the trailing edge and the ground by the chord length is defined as h/C. The size of the computational domain is $-7C \le x \le 10C$ and $-h \le y \le 7C$ for the streamwise and vertical directions, respectively.

A no-slip boundary condition is imposed on the surface of the wing while the symmetry condition is set for the far-field boundary. A uniform flow with the free-stream velocity (U_∞) and low turbulent intensity and the convective condition are applied on the inflow and outflow boundaries, respectively. The moving wall boundary with free-stream velocity is specified at the ground surface. The minimum vertical grid spacing on both the wing and the ground surface is chosen about $10^{-3}C$ corresponding to $y^+ \approx 50$ as wall unit at the same Reynolds number ($\mathrm{Re} = U_\infty C / \nu$) of 2×10^6 considered in this study.

In order to capture accurately the separating shear layers on both the wing and the ground, the grids are distributed non-uniformly near these regions, especially in the gap and the wake regions. To consider the variation of ground clearance, dense resolutions near both of the wing and the ground surface and area under the wing are maintained. Fig. 1(b) shows the typical grid distribution near the wing at the angle of attack of $0°$ for the ground clearance of 0.1 and the ground surface. In order to consider the variation of the gap ratio, the number of grid points used in the y direction is tuned to maintain the dense resolution near the wing, moving wall and in the gap spacing. The grid-dependency study has been confirmed with the coarse, medium and fine grids of 1.5×10^4 (grid-A), 3×10^4 (grid-B) and 4.5×10^4 (grid-C), respectively. Table 1 shows the lift, drag coefficients for the different grid sets. The comparison indicates that the similar results are given by grid-B and grid-C. Therefore, grid-B is seen to be reasonable for flow predictions and it will be used for the following calculation.

(a)   (b)
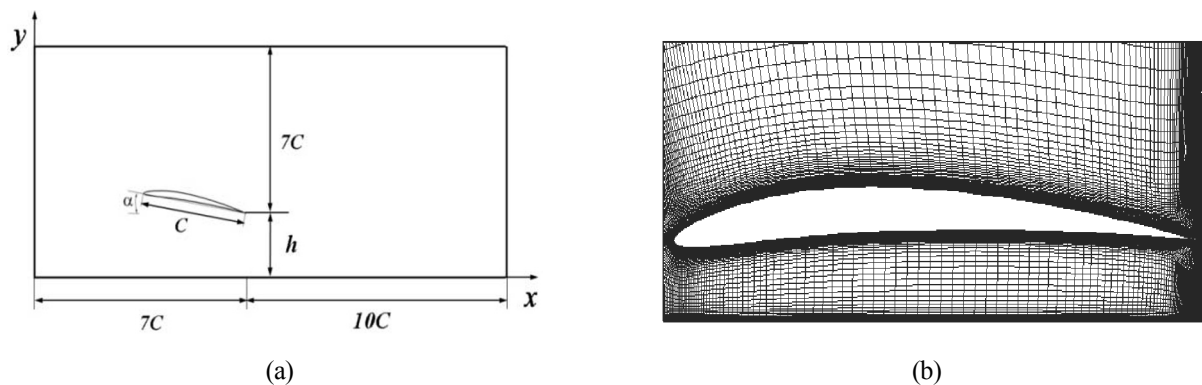
Fig. 1 (a) Physical model of 2-D WIG problem, the computational domain and coordinate system, and (b) typical grid system near the wing and ground for $\alpha = 0°$.

Table 1 Grid-dependency study for NACA4406 at $\alpha = 2°$ and $h/C = 0.1$.

	Grid-A	Grid-B	Grid-C
C_l	0.8408	0.8411	0.8414
C_d	0.00993	0.00977	0.00976

The dependence of the present problem of two-dimensional steady flow around NACA profiles in ground effect on the turbulence model has been investigated to justify the realizable $k-\varepsilon$ model employed in this study. The two-equations models of $k-\varepsilon$ type have been popularly and successfully employed to the practical problems assumed as the steady flow. Thus, two different models of standard and realizable $k-\varepsilon$ models are considered to simulate the flow around NACA 4406 at $\alpha = 2°$ and $h / C = 0.1$ in order to testify the dependence on the turbulence model. The lift coefficients of two different models have been compared in Fig. 2. The standard model doesn't predict stall, meaning that lift coefficient increases over the range of the angle of attack except the highest angle of $30°$. However, the realizable $k-\varepsilon$ model gives more reasonable result which represents stall. This comparison supports the improved predictive capabilities of the realizable $k-\varepsilon$ model compared to the standard $k-\varepsilon$ model and its ability to resolve portions of complex flows located very close to the surface. Consequently, the realizable $k-\varepsilon$ model is selected in this study.

Validation of the present computational method is performed for two different 2-D wings of NACA 0006 and 4406 at $\alpha = 2°$ and $h / C = 0.1$. Fig. 3 shows the distribution of the mean pressure coefficient $(\overline{C}_p)$ on the wing surfaces compared with the results of Moon, Oh and Seo (2005). The predicted $\overline{C}_p$ distributions agree very well with those of Moon, Oh and Seo (2005), indicating the adequacy of the present method for the analysis of turbulent flow in the WIG problem. The additional simulations were carried out for the isolated NACA 0015 in the range of $0° \le \alpha \le 24°$ at the Reynolds number of 8.96×10^5. The two-dimensional results of the present study and Duvigneau and Visonneau's computation (2006) agree well with the force measurements of Gilarranz, Traub and Rediniotis (2002) before stall as shown in Fig. 4.
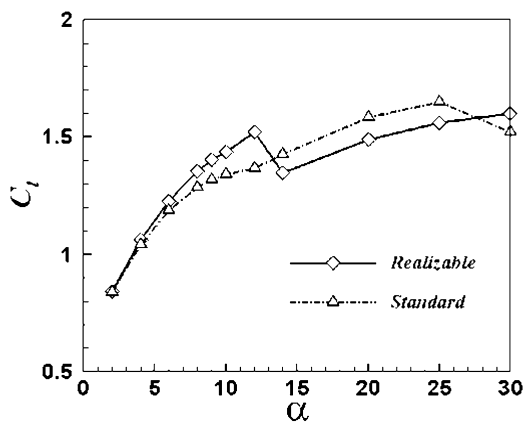
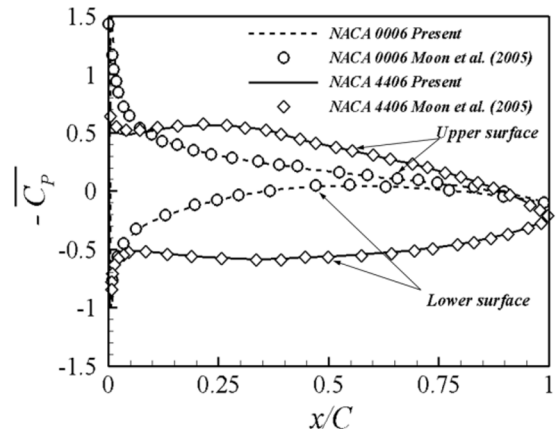Fig. 2 Lift coefficients of the standard and realizable $k-\varepsilon$ models.

Fig. 3 Distributions of mean pressure coefficient on the surface of NACA0006 and 4406 for $\alpha = 2°$ and $h / C = 0.1$.
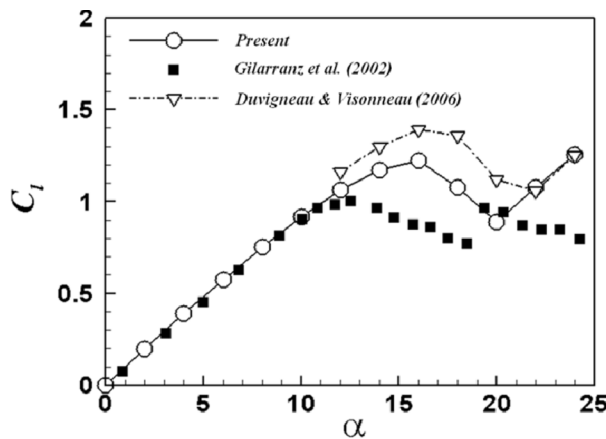
Fig. 4 Lift coefficients as a function of the angle of attack for the isolated NACA 0015 at the Reynolds number of 8.96×10^5

However, after stall occurs experimentally at the angle of attack of about 12°, the differences between the two-dimensional simulations and the experiment appear. These differences are attributed to inherent unsteady thee-dimensionality in the flow originated by the relatively large and highly complex vortical structures separated from the leading edge, which cannot be accurately resolved with a two-dimensional model. This hardness to accurately simulate the post-stall regime was pointed out by the several authors such as Ravindran (1999).

Even though two-dimensional results of the present study and Duvigneau and Visonneau's computation (2006) show the delay of stall and the difference of the magnitude in the post-stall regime, forces according to the angle of attack reveal the similar pattern that the magnitude drops after stall and then increases. However, from these results in Fig. 4, it is concluded that the present simulations under the assumption of the two-dimensional steady turbulence are more suitable for the pre-stall region. Thus, the present study focused on the mean flow characteristics in pre-stall regime of $0° \leq \alpha \leq 10°$.

AIRFOIL PROFILE SELECTION

The present study considers five different 2-D wings of the same 4-digit family with a maximum deflection of camber of 4% of the chord, and the maximum camber is located at 40% of the chord. The aim of this preliminary test is to select a profile with the highest value of lift-to-drag ratio.

The five profiles of NACA 4406, 4409, 4412, 4415 and 4418 are depicted in Fig. 5. Eventually, the profiles are tested at $\alpha = 2°$ and $h/C = 0.1$ for $Re = 2 \times 10^6$ with the incoming turbulent intensity of 0.1% to select a profile with the highest value of lift-to-drag ratio.

Table 2 shows the lift and drag coefficients for the five airfoils. The lift is found to be higher for the profiles with smaller thicknesses. The maximum lift coefficient of about 0.84 is found for NACA 4406; while for the largest thickness profile of
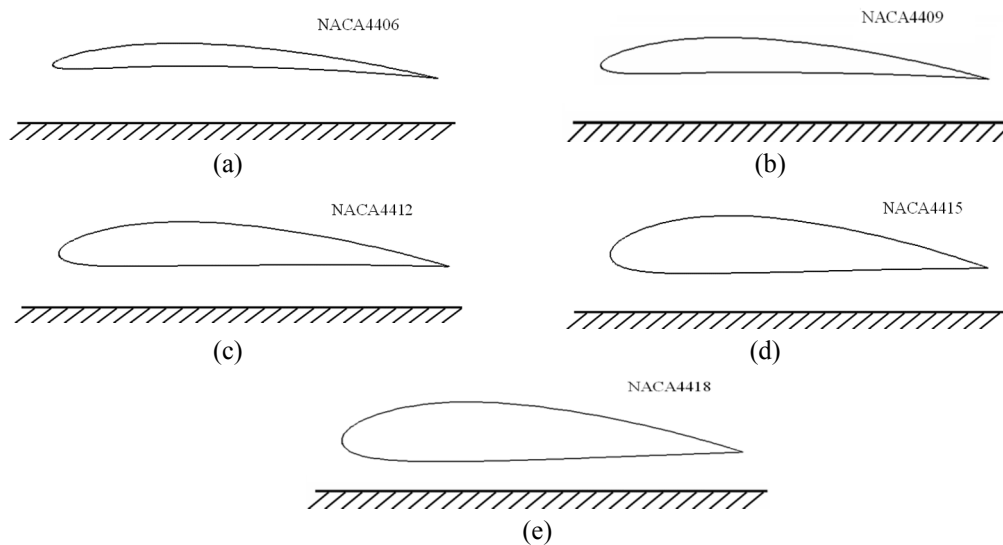
Fig. 5 Profiles of five different 2-D airfoils in ground effect.

Table 2 Aerodynamic characteristics of 2-D wings in ground effect.

NACA	C_l			C_d		
	Present	Moon, Oh and Seo (2005)	Hsiun and Chen (1995)	Present	Moon, Oh and Seo (2005)	Hsiun and Chen (1995)
4406	0.841	0.853		0.00990	0.00929	
4409	0.796	0.805	0.611	0.01070	0.00986	0.01857
4412	0.722	0.727	0.488	0.01190	0.01080	0.02714
4415	0.605			0.01360		
4418	0.429			0.01620		

NACA 4418, a lift coefficient of nearly 0.43 is obtained. The drag coefficient increases when the thickness is increased. The trend of the lift and drag coefficients according to the profiles is similar to that of the previous numerical studies of Hsiun and Chen (1995) and Moon, Oh and Seo (2005) and Loftin and Smith's (1949) experiment. A comparison of the lift-to-drag ratios indicates that the NACA 4406 gives the best aerodynamic performance with a lift-to-drag ratio of about 86.

RESULT AND DISCUSSION

The profile of NACA 4406 has been selected for the 2-D WIG problem, based on the aerodynamic examinations of five different profiles. Regarding NACA 4406, the 2-D WIG problem will be investigated at six different ground clearances of 0.1, 0.25, 0.5, 0.75, 1.0 and 1.25 for different angles of attack ranging from $0°$ to $10°$. The flow is at $Re = 2 \times 10^6$ and has the incoming turbulent intensity of 0.1%.

Flow and pressure distribution on the wing

The mean streamlines around the wing at $h/C = 0.1$ for different angles of attack of $\alpha = 0°$, $4°$, $8°$ and $10°$, respectively, are shown in Figs. 6(a-d). In the range of $0° \leq \alpha \leq 10°$ at the lowest $h/C = 0.1$ among the ground clearances considered in this study, the mean flow is almost the same pattern as the streamlines that follow the wing surface, except where the stagnation point gradually moves from the leading edge to the lower surface with increasing the angle of attack as shown in Figs. 6(a-d).
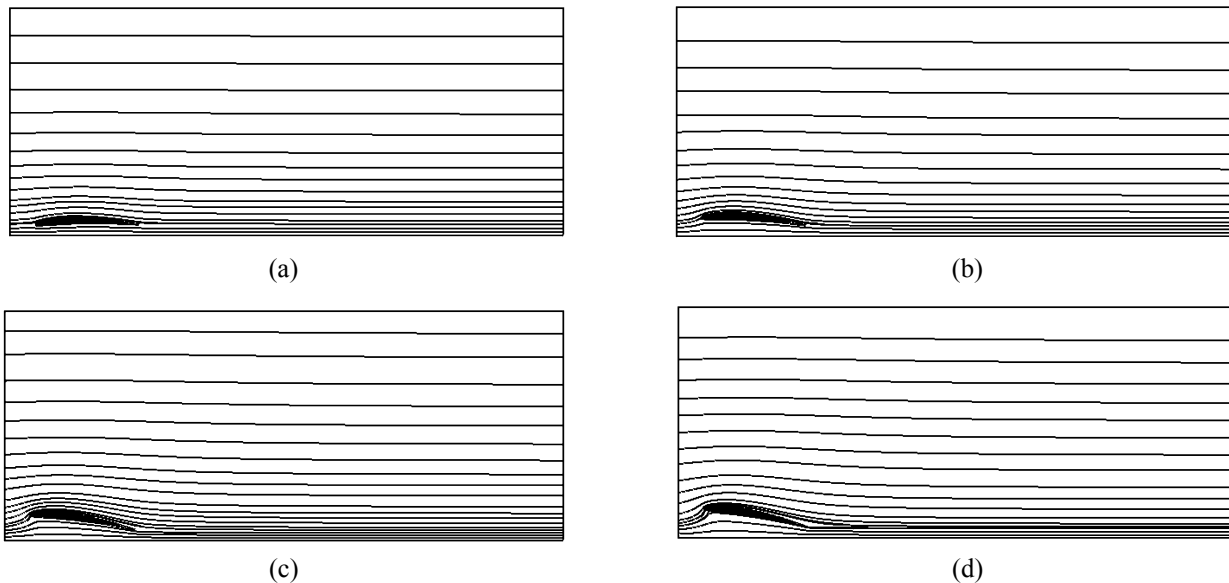

Fig. 6 Mean streamlines around the wing at $h/C = 0.1$ for (a) $\alpha = 0°$, (b) $\alpha = 4°$, (c) $\alpha = 8°$, (d) $\alpha = 10°$.

In the range of $0° \leq \alpha \leq 10°$, the dependence of the mean flow on the h/C is very weak. Therefore, the pattern of mean flow for different h/C s is very similar for the corresponding α as shown in Figs. 6(a-d) (though not shown here for sake of brevity).

Fig. 7 shows the variation of the mean pressure coefficient $(\overline{C_p})$ on the wing surface at different h/C s for four different angles of attack of $0°$, $4°$, $8°$ and and $10°$. In the case of $\alpha = 0°$, near the leading edge, the suction and pressure effects occur on the lower and the upper surfaces, respectively, regardless of h/C. Consequently, in this region, the pressure on the upper surface is higher than that on the lower surface, which means that the value of $-\overline{C_P}$ on the lower surface is larger than that of $-\overline{C_P}$ on the upper surface as shown in Fig. 7(a). After passing the region near the leading edge, the pressure distribution undergoes the opposite trend to that near the leading edge, resulting in a higher pressure on the lower surface than on the upper surface. Since the cambered wing has a high flow divergence, the higher pressure is distributed on the lower surface through the chord length, except for the area close to the leading edge.

When the angle of attack is imposed on the wing, the distribution of $\overline{C_P}$ is considerably changed from that of $\overline{C_P}$ for $\alpha = 0°$, especially near the leading edge, as shown in Figs. 7(b-d). However, in the range of $0° \leq \alpha \leq 10°$, it can be demonstrated from Figs. 7(b-d) that a similar pattern of $\overline{C_P}$ variation occurs along the wing surface according to h/C, which can be supported by the similar flow pattern observed in Figs.6 (b-d).

On the upper surface, in the proximity of the leading edge, the pressure becomes very low because the suction effect becomes strong as the stagnation point moves toward the lower surface with increasing α. Namely, the high positive value of $-\overline{C_P}$ appears in the proximity of the leading edge as shown in Figs. 7(b-d). As we move toward the trailing edge on the upper surface, the pressure augments. At the fixed α, with increasing h/C, the pressure on the upper surface slightly reduces. This reduction rate of pressure according to h/C increases with increasing α.

On the lower surface, the pressure changes rapidly from the low state to the high state in the proximity of the leading edge, corresponding with the positive value of $-\overline{C_P}$ decreasing quickly with the negative value of $-\overline{C_P}$. After the pressure reaches the maximum in the proximity of the leading edge on the lower surface, it slightly decreases. As α increases, the location of the maximum pressure corresponding to the negative peak of $-\overline{C_P}$ becomes more distant because the stagnation point moves toward the lower surface, which can be clarified by comparing Figs. 7(b-d). At a fixed α, with increasing h/C, especially in the range of $0.1 \leq h/C \leq 0.75$, the pressure on the lower surface clearly decreases. However, further increasing h/C from 0.75 to 1.25, the variation of pressure on the lower surface is not considerable.
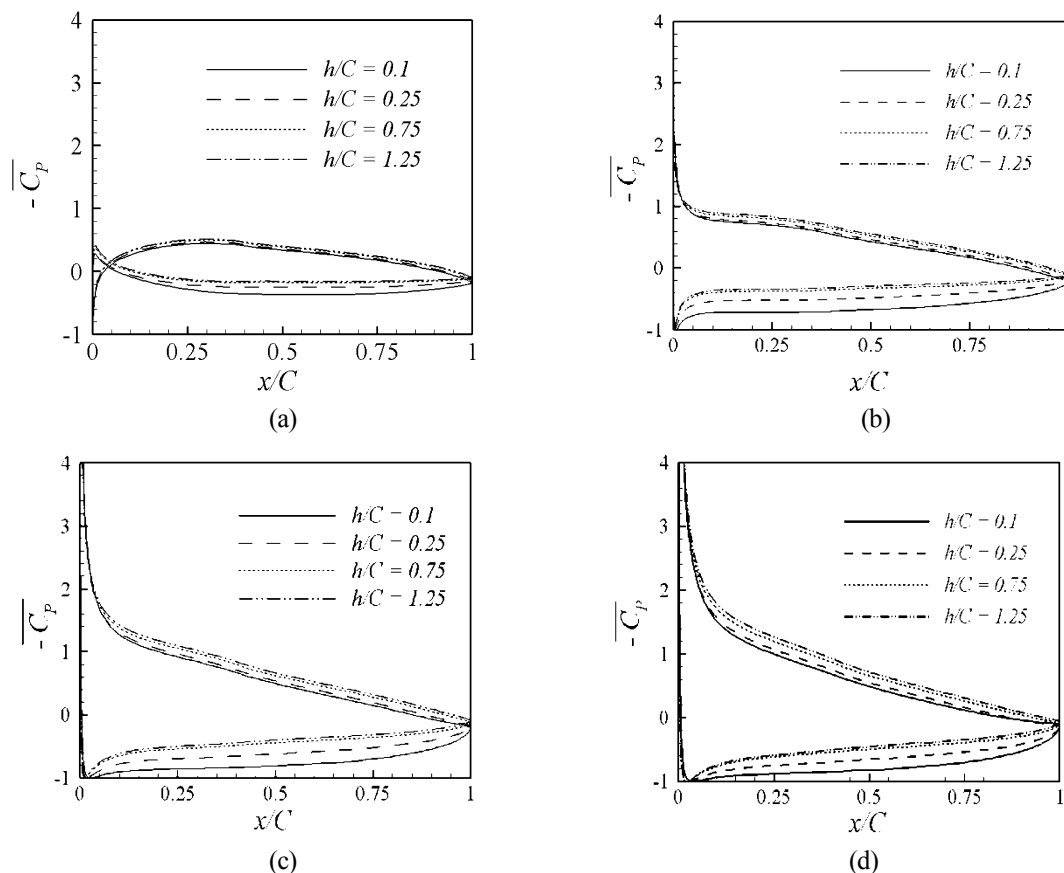

Fig. 7 Distribution of pressure coefficient on the surface of wing for different ground clearances at (a) $\alpha = 0°$, (b) $\alpha = 4°$, (c) $\alpha = 8°$ and (d) $\alpha = 10°$.

Force coefficients

Fig. 8 shows the lift coefficient (C_l) as a function of h/C for different angles of attack. In the range of $0° \leq \alpha \leq 10°$, the dependence of C_l on h/C is generally the same as follows. The maximum C_l occurs at the lowest h/C of 0.1 and then C_l decreases with increasing h/C. Finally, C_l almost saturates when h/C reaches 0.75. At the fixed h/C, C_l shows an augmenting behavior as α increases. The decrease rate of C_l reduces with increasing α as shown in Fig. 8.
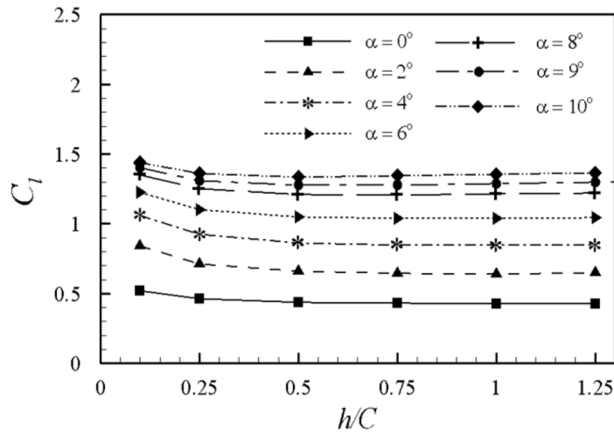
Fig. 8 Lift coefficient as a function of the ground clearance for different angles of attack in the range of $0° \leq \alpha \leq 10°$.
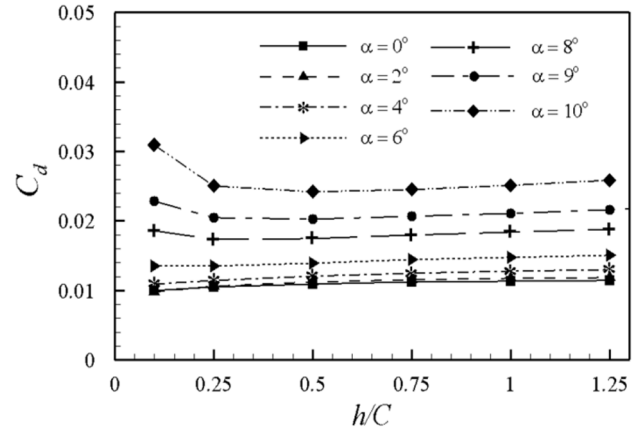

Fig. 9 Drag coefficient as a function of the ground clearance for different angles of attack in the range of $0° \leq \alpha \leq 10°$.
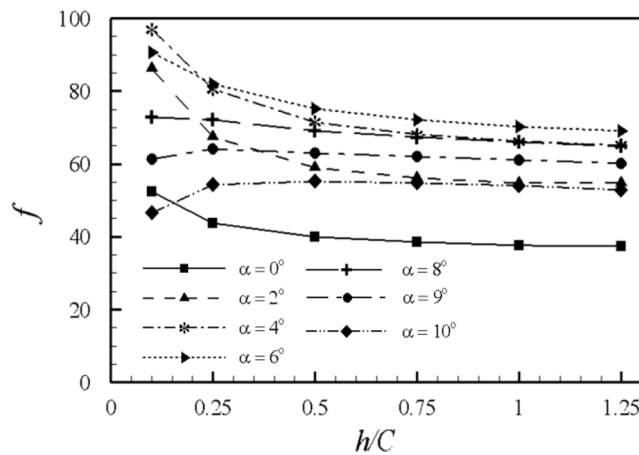

Fig. 10 Lift-to-drag ratio as a function of the ground clearance for different angles of attack in the range of $0° \leq \alpha \leq 10°$.

The drag coefficient (C_d) as a function of h/C for different angles of attack is plotted in Fig. 9. At the fixed α in the range of $0° \leq \alpha \leq 6°$, C_d slightly increases with increasing h/C as shown in Fig. 9. For $\alpha = 8°$, 9° and 10°, C_d has a maximum at the lowest h/C of 0.1 and then it decreases at $h/C = 0.25$. Over $h/C = 0.25$, the values of C_d are almost the same for the cases of $\alpha = 8°$, 9° and 10°. At the fixed h/C, C_d shows an increasing behavior as α increases. In contrast to C_l shown in Fig. 8, the decrease rate of C_d corresponding to h/C augments with increasing α in the range of $0° \leq \alpha \leq 10°$ as shown in Fig. 9. In order to investigate the aerodynamic performance, the lift-to-drag ratio ($f = C_l / C_d$) as a function of the ground clearance for different angles of attack, is depicted in Fig. 10.

The behavior of f for the ground clearances and the angles of attack can be estimated from C_l and C_d as shown in Figs. 8 and 9, respectively. A comparison of the lift-to-drag ratios indicates that the best aerodynamic performance with a lift-to-drag ratio of about 97 is obtained at $\alpha = 4°$ and $h/C = 0.1$. Generally, with the exception of the lowest h/C, the smallest f at the corresponding h/C appears at $\alpha = 0°$. It is interesting to note that the case of $\alpha = 6°$ reveals the highest f over the h/C range, except for the lowest h/C.

Effect of Reynolds number

For $Re = 2 \times 10^6$, the evaluation of aerodynamic characteristics for 2-D WIG of NACA 4406 in the wide ranges of ground clearances and angles of attack indicated that the best aerodynamic performance with the highest value of the lift-to-drag ratio is obtained at $\alpha = 4°$ and $h/C = 0.1$. Thus, under the conditions of $\alpha = 4°$ and $h/C = 0.1$, the effect of the Reynolds

number on the aerodynamic characteristics such as the distribution of $\overline{C_P}$ and force coefficients for 2-D WIG of NACA 4406 is investigated in the range of $2 \times 10^5 \leq \text{Re} \leq 2 \times 10^9$.

Fig. 11 shows the variation of the mean pressure coefficient on the wing surface at $\alpha = 4°$ and $h/C = 0.1$ for different Reynolds numbers. Regardless of Re, the distribution of $\overline{C_P}$ on the wing surface is analogous to that of $\text{Re} = 2 \times 10^6$ as previously shown in Fig. 7(b).

Consequently, over the entire range of the chord length, the pressure on the lower surface is higher than that on the upper surface, which means that the value of $-\overline{C_P}$ on the upper surface is larger than that of $-\overline{C_P}$ on the lower surface as shown in Fig. 11. On the upper surface, as Re increases, the pressure becomes lower. In contrast, on the lower surface, the pressure becomes higher with increasing Re. This dependency of pressure on Re is more distinguished as we move to the trailing edge.

Fig. 12 shows the drag and lift coefficient and the lift-to-drag ratio as a function of the Reynolds number. As shown in Fig. 12(a), C_l augments rapidly with increasing Re and eventually for $\text{Re} \geq 2 \times 10^8$ the variation of this value is very small. In contrast to C_l, the value of C_d diminishes rapidly with increasing Re and when further increasing $\text{Re} \geq 2 \times 10^8$, this value tends to be converged as shown in Fig. 12(b). As Re increases, the lift-to-drag ratio increases linearly as shown in Fig. 12(c). The increment of f is governed by the linear function of $f \sim a \cdot \text{Re}$, where α is the slope with the value of about 66.
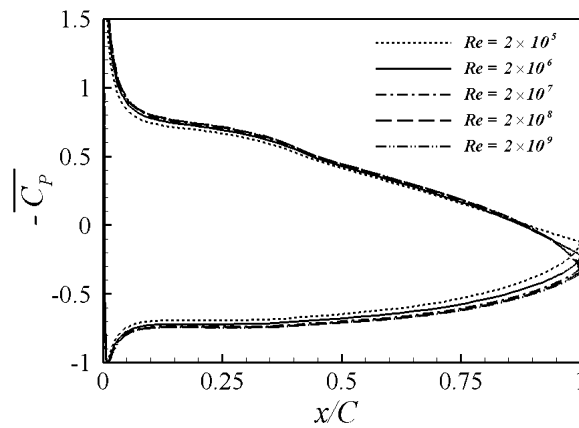

Fig. 11 Distribution of pressure coefficient on the surface of wing for different Reynolds numbers at $\alpha = 4°$ and $h/C = 0.1$.
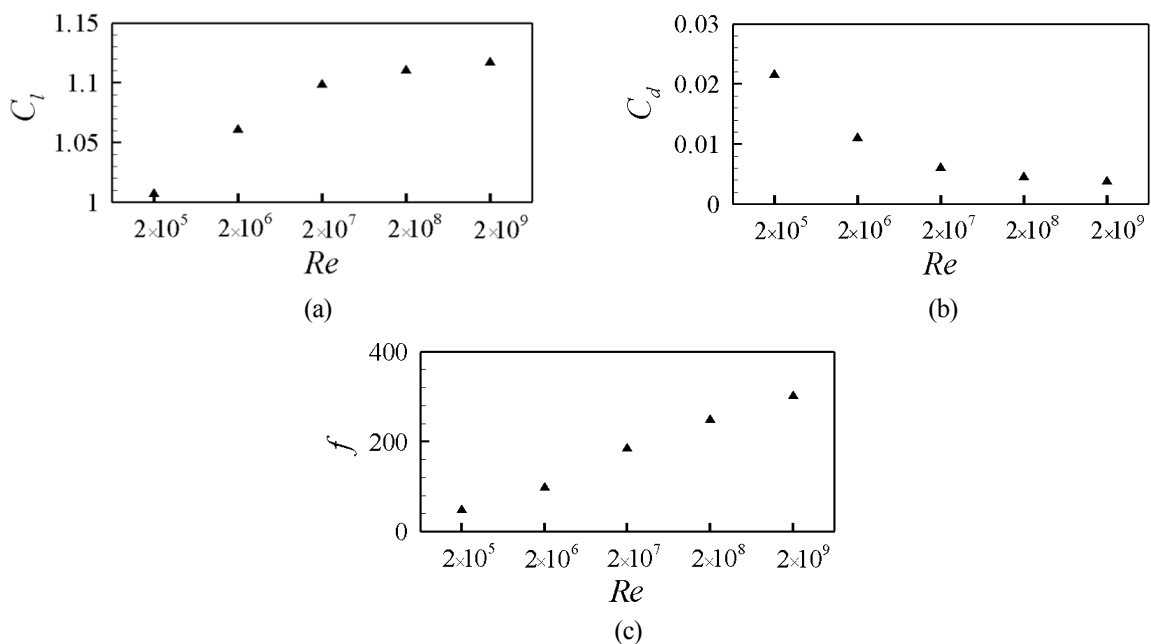

Fig. 12 (a) Lift coefficient, (b) drag coefficient and (c) lift-to-drag ratio as function of Reynolds number.

CONCLUSIONS

The present study considered the two-dimensional WIG (Wing in ground) problem with the assumption of the steady incompressible viscous flow in order to simplify the physical problem. The commercial CFD package, FLUENT (2009), is employed for all numerical predictions. The flow characteristics of a cambered airfoil of NACA 4406 have been numerically studied at various ground clearances ($0.1 \leq h/C \leq 1.25$) for $0° \leq \alpha \leq 10°$ at $Re = 2 \times 10^6$.

In the range of $0° \leq \alpha \leq 10°$, the mean flow showed almost the same pattern without the flow separation. However, the stagnation point slightly moved from the leading edge to the lower surface with an increasing angle of attack. In general, the higher pressure is distributed on the lower surface through the chord length because the cambered wing has a high flow divergence regardless of the angle of attack.

For all the angles of attack considered in this study, the variation of C_l and C_d was negligible over a certain distance from the ground. The maximum lift-to-drag ratio (C_l / C_d) was achieved at $\alpha = 4°$ and $h/C = 0.1$.

The study on the effect of the Reynolds number on the aerodynamic characteristics of NACA 4406 for $\alpha = 4°$ and $h/C = 0.1$ showed that C_l and C_d increased and decreased, respectively, with increasing Re in the range of $2 \times 10^5 \leq Re \leq 2 \times 10^9$. The dependency of C_l and C_d on the Reynolds number was significant in low Reynolds numbers. The lift-to-drag ratio increases linearly with an increasing Reynolds number. Although the present study does not consider the wide range of ground clearances and angles of attack, it raises the understanding of the ground effect at a high Reynolds number.

REFERENCES

Ahmed , N.A. and Goonaratne, J., 2002. Lift augmentation of a low-aspect-ratio thick wing in ground effect. *Journal of Aircraft*, 39(2), pp.381-384.

Ahmed, M.R. and Sharma, S.D., 2005. An investigation on the aerodynamics of a symmetrical airfoil in ground effect. *Experimental Thermal and Fluid Science*, 29(6), pp.633-647.

Chun, H.H. and Chang, C.H., 2002. Longitudinal stability and dynamic motions of a small passenger WIG craft. *Ocean Engineering*, 29(10), pp.1145-1162.

Chun, H.H., Chang, J.H., Paik, K.J. and Chang, S.I., 1997. Preliminary design of a 20 passenger PARWIG craft and construction of a 1/10 scale radio controlled model. *Proceeding of International Conference on FAST Sea Transportation*. Sydney, Australia, pp.513-520.

Duvigneau, R. and Visonneau, M., 2006. Optimization of a synthetic jet actuator for aerodynamic stall control. *Computers and Fluids*, 35(6), pp.624-638.

Fink, P.M. and Lastinger, L.J., 1996. *Aerodynamics Characteristics of Low-Aspect-Ratio Wings in Close Proximity to the ground*. NASA TN D-926.

Fluent Inc, 2009. *Fluent user's guide version 12*.0.3: Fluent Inc, Lebanon.

Gilarranz, J., Traub, L. and Rediniotis, O., 2002. *Characterization of a compact, high power synthetic jet actuator for flow separation control*. AIAA paper. 0127.

Han, C., Cho, L. and Cho, J., 2005. Wake Shapes Behind Wings in Close Formation Flight Near the Ground. *Journal of Mechanical Science and Technology*, 19(2), pp.674-681.

Hsiun, C.M. and Chen, C.K., 1995. Numerical investigation of the thickness and camber effects on aerodynamic characteristics for two-dimensional airfoils with ground effect in viscous flow. *Transactions of the Japan society for aeronautical and space sciences*, 38(119), pp.77-90.

Hsiun, C.M. and Chen, C.K., 1996. Aerodynamic characteristics of a two-dimensional airfoil with ground effect. *Journal of Aircraft*, 33(2), pp.386-392.

Kim, S.K., Suh, S.B., Lee, D.H. and Kim, K.E., 1997. Wind tunnel test study on the wings of WIG ship. *Journal of the Society of Naval Architects of Korea*, 34(1), pp.60-67.

Kim, Y., Lee, J.E., Shin, M.S., Kang, K.J. and Kwon, J.H., 2006. Turbulent flow simulation on the ground effect about a 2-dimensional airfoil. *Journal of computational fluids engineering*, 11(4), pp.81-89.

Launder, B.E. and Spalding, D.B., 1974. The Numerical Computation of Turbulent Flows. *Computer Methods in Applied Mechanics and Engineering*, 3(2), pp.269-289.

Loftin, L.K. and Smith, H.A., 1949. *Aerodynamic characteristics of 15 NACA airfoil sections at seven Reynolds numbers from* 0.7×10^6 *to* 9.0×10^6. NACA Technical Note 1945.

Moon, Y.J., Oh, H.J. and Seo, J.H., 2005. Aerodynamic investigation of three-dimensional wings in ground effect for aero-levitation electric vehicle. *Aerospace Science and Technology*, 9(6), pp.485-494.

Muzitani, N. and Suzuki, K., 1993. Numerical Analysis of 3-D WIG Advancing over Still Water Surface. *Journal of the Society of Naval Architects of Japan*, 174, pp.35-46.

Nuhait, A.O. and Mook, D.T., 1989. *Numerical Simulation of Wings in Steady and Unsteady Ground Effects*. *Journal of aircraft*, 26(12), pp.1081-1089.

Raymond, A.E., 1921. *Ground influence on aerofoil*. NACA Technical Note 67.

Ravindran, S., 1999. *Active control of flow separation over an airfoil*. Technical Report TM-1999-209838, NASA.

Recant, I.R., 1939. *Wind-tunnel investigation of ground effect on wings with flap*. NACA Technical Note 705.

Reid, E.G., 1927. *A full-scale investigation of ground effect*. NACA Technical Report 625.

Seerebrisky, Y.M., 1946. *Wind-tunnel investigation of the horizontal motion of a wing near the ground*. NACA Technical Note 1095.

Shin, M.S., Yang, S.I., Joo, Y.R., Kim, S.K., Bae, Y.S., Kim, J.H. and Chun, H.H., 1997. Wind tunnel test results for eight and twenty passenger class WIG effect ships. *Proceeding of International Conference on FAST Sea Transportation*. Sydney, Australia, pp.565-570.

Zerihan, J. and Zhang, X., 2000. Aerodynamics of a single element wing in ground effect. *Journal of Aircraft*, 37(6), pp. 1058-1064.

Zhang, X., Zerihan, J., Ruhrmann, A. and Deviese, M., 2002. Tip vortices generated by a wing in ground effect. *In: Proceedings of the 11th International Symposium on Applications of Laser Techniques to Fluid Mechanics*. Lisbon, Portugal.